Accepted Manuscript

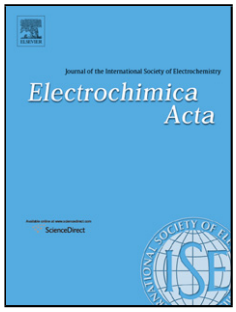

Title: Comparison of the Spinels Co_3O_4 and $NiCo_2O_4$ as Bifunctional Oxygen Catalysts in Alkaline Media

Author: Derek Pletcher Xiaohong Li Stephen W.T. Price Andrea E. Russell Turgut Sönmez Stephen J. Thompson

PII: S0013-4686(15)30601-0
DOI: http://dx.doi.org/doi:10.1016/j.electacta.2015.10.020
Reference: EA 25823

To appear in: *Electrochimica Acta*

Received date: 19-8-2015
Revised date: 7-9-2015
Accepted date: 5-10-2015

Please cite this article as: Derek Pletcher, Xiaohong Li, Stephen W.T.Price, Andrea E.Russell, Turgut Sönmez, Stephen J.Thompson, Comparison of the Spinels Co3O4 and NiCo2O4 as Bifunctional Oxygen Catalysts in Alkaline Media, Electrochimica Acta http://dx.doi.org/10.1016/j.electacta.2015.10.020

Comparison of the Spinels Co_3O_4 and $NiCo_2O_4$ as Bifunctional Oxygen Catalysts in Alkaline Media

Derek Pletcher,[1a] Xiaohong Li[b], Stephen W.T. Price,[1c] Andrea E. Russell,[1a]*

Turgut Sönmez[1a] and Stephen J. Thompson[1a]

[a] Chemistry, University of Southampton, Southampton SO17 1BJ, UK

[b] Renewable Energy Group, College of Engineering, Mathematics and Physical Sciences, University of Exeter, TR10 9FE, UK

[c] Diamond Light Source Ltd, Diamond House, Harwell Science and Innovation Campus, Didcot, Oxfordshire, OX11 0DE

[1] ISE member

*a.e.russell@soton.ac.uk

ABSTRACT

Data from experiments with both rotating disc electrodes (RDEs) and gas diffusion electrodes (GDEs) are used to investigate the properties of the spinels, Co_3O_4 and $NiCo_2O_4$, as bifunctional oxygen electrocatalysts. Emphasis is placed on catalyst compositions and electrode structures free of carbon. Oxygen evolution and reduction occur at surfaces where the transition metals are in different oxidation states but the surface can be repeatedly cycled between these two states without significant change. It is shown that carbon-free, $NiCo_2O_4$ catalysed GDEs can be fabricated using structures based on stainless steel cloth or nickel foam. Those based on nickel foam can be cycled extensively and allow both O_2 evolution and reduction at current densities up to 100 mA cm^{-2}.

Keywords: Oxygen evolution; oxygen reduction; alkaline; spinel; gas diffusion electrode.

1. Introduction

Electrocatalysts that can support both oxygen reduction and oxygen evolution at high current densities are critical components of proposed metal/air secondary batteries and reversible fuel cells. Spinels have been widely proposed as bifunctional oxygen electrocatalysts in alkaline media [1-6], but their performance at practical current densities is seldom reported. One reason is that to operate as a bifunctional electrode at high current densities, the electrocatalyst must be placed into a GDE structure that allows both a high flux of O_2 to the catalyst sites during battery discharge and effective removal of O_2 away from these sites during battery charge. Dispersal of the gas away from the interelectrode gap, ie. into the gas space behind the catalyst layer is much preferable. Moreover, this performance must be achieved with a GDE without carbon components since carbon is prone to corrosion in strong alkali at the potentials for oxygen evolution, particularly at elevated temperatures [7-11].

Our target is the design of an electrode free of both precious metal and carbon powder that supports both oxygen reduction and oxygen evolution at high current densities. Spinels, especially Co_3O_4 and $NiCo_2O_4$ have been selected as non-precious metal catalysts for such electrodes [12-14] and this paper compares the performance of these two oxides as a bifunctional oxygen electrocatalyst. The comparison is based on experiments with RDE and the paper also contains performance data for GDE based on the preferred catalyst.

2. Experimental

2.1 Catalyst Preparation

The preparation of the two spinels was described in the previous paper[14]; characterisation of the spinel powders using XRD, SEM, TEM and surface area determination is presented in the Supplementary Information to the paper [14]. Pt black (Fuel Cell Grade) was purchased from E-TEK.

2.2 Instrumentation

All electrochemical experiments were carried out with Autolab PGSTAT instruments with NOVA and GPES software packages. The rotation rates of the electrodes were controlled by Pine Instrument Rotators, type CPR or MSR.

2.3 Electrochemical Cells and Electrolyte

Experiments were carried out in beaker cells (volume ~ 200 cm^3) with a polymer cover and a water jacket. Water, temperature controlled with a Grant TC120 recirculator with a 5 litre reservoir, was passed through the jacket. The counter electrode was a Pt gauze in the same compartment and the reference electrode a laboratory fabricated Hg/HgO/KOH electrode inside a Luggin capillary. The KOH concentration in the reference electrode was always the same as used in the solution under study. With 1 M KOH, the potential of the reference electrode is + 866 mV vs NHE.

For experiments with disc electrodes, the working electrode was a 0.2 cm^2, glassy carbon disc electrode (Pine Instruments AF3M electrode) coated with a catalyst layer without

carbon powder applied as an ink. To prepare the ink, 2 mg catalyst in 6 cm^3 of deionised water was placed in an ultrasonic bath (Fisherbrand FB15046) for 30 minutes followed by 2 minutes shear force stirring in a homogeniser (Fisher Powergen 1000). The ink was applied to pre-polished (with alumina slurries of 1.0 μm then 0.05 μm particle size on a microcloth), glassy carbon discs in 3 x 15 μl aliquots with drying with an IR heat lamp between applications. Finally, a thin film of Nafion was drop cast over the catalyst layer using 15 μl of 1 wt % Nafion in water (prepared from aqueous Nafion solution, 10 % solids (Ion Power GmbH)) and the coating again dried. This final layer was found to greatly enhance the stability of the coating and improve the reproducibility of experimental data. The final catalyst loading on the glassy carbon disc was 75 μg cm^{-2}.

The gas diffusion electrodes (GDEs) were based on 12 mm diameter discs that were mounted inside a PTFE holder so that the $NiCo_2O_4$/PTFE layer was adjacent to the electrolyte and an area of 0.5 cm^2 was exposed to both electrolyte and gas phase. Electrical contact was made with a fine Ni mesh and Ni wire on the gas side. Oxygen gas was passed to the rear of the GDE with a feed rate of 3.3 cm^3 s^{-1} controlled via a flowmeter. Two types of GDE were fabricated:

(a) *Steel cloth collector* – Discs (diameter 12 mm) were cut from a stainless steel filter cloth (Type BMT50 - United Wire Ltd) and cleaned. They were placed in acetone in an ultrasonic bath (Fisherbrand FB15046) for 20 minutes, acid etched in 1 M HCl, washed well with water and dried. $NiCo_2O_4$ powder (100 mg), and 60 % PTFE solution (50 mg) were mixed with isopropanol (0.2 cm^3) and water (1 cm^3). For some GDEs, sodium sulphate (10 mg) was added as a pore-former. The mixture was then ultrasonicated for 20 minutes and homogenised (Fisher Powergen 1000) for 2 minutes to form an ink with a ratio of $NiCo_2O_4$: PTFE of 10:3 by mass. The ink was then sprayed onto the steel cloth with an airgun (Iwata

CM-B spray-gun) and dried with a hot air gun. The spray coating was repeated to obtain the desired loading with the cloth heated by a hot air-gun between catalyst-film applications. The electrodes were then compressed with a pressure of 4 kg cm^{-2} at a temperature of 450 K for 5 minutes. Finally, the whole structure was dipped three times into a solution of 2 M $Co(NO_3)_2$ + 1 M $Ni(NO_3)_2$ for 5 minutes with drying between dips before heating to 648 K for 3 hours. While not essential, the final in situ deposition of a $NiCo_2O_4$ layer was found to improve reproducibility of the GDE performance. The treatment probably led to protection of the stainless steel surface and certainly the heat treatment led to PTFE migration through the structure and consequent improvement in catalyst adhesion to the cloth, as well as increased hydrophobicity and/or increased porosity to gas. The final $NiCo_2O_4$ loading was 10 - 20 mg cm^{-2}.

(b) *Ni foam current collector* - Discs (diameter 12 mm) cut from a nickel foam sheet (thickness 1.9 mm, 20 pores/cm – Goodfellow Metals) were first cleaned. They were ultrasonicated in acetone for 20 minutes, acid etched in 1 M HCl at 353 K for ~ 1 hour and then washed with water and ultrasonicated in water for 15 minutes. $NiCo_2O_4$ powder (150 mg), and 60 % PTFE solution (75 mg) were mixed with isopropanol (0.5 cm^3) and water (0.5 cm^3). The paste was then ultrasonicated for 20 minutes and homogenised for 4 minutes to form an ink before drying to a paste with a ratio of $NiCo_2O_4$: PTFE of 10:3 by mass. The $NiCo_2O_4$/PTFE paste (200 mg wet weight ~ 120-150 mg dry weight) was spread uniformly over the Ni foam disc and pressed in a Specac hydraulic press at 1.5 kN cm^{-2} and 298 K for 30 s. As with the stainless steel cloth GDEs, in a final stage, the whole structure was dipped three times into a solution of 2 M $Co(NO_3)_2$ + 1 M $Ni(NO_3)_2$ for 5 minutes with drying between dips before heating to 648 K for 3 hours.

3. Results

3.1 Oxidation States in the Spinel

Figure 1 shows cyclic voltammograms for Co_3O_4 and $NiCo_2O_4$ coated glassy carbon disc electrodes in 1 M KOH at 298 K, recorded with a potential scan rate of 10 mV s^{-1} between the potentials for oxygen evolution and reduction. The dominant features on the forward scans are well-formed oxidation peaks at slightly less positive potentials than that for O_2 evolution. Nickel, cobalt and mixed Ni/Co oxides/hydroxides all show such peaks and they are generally attributed to a change in oxidation state of Ni/Co ions in the lattices. The peak for $NiCo_2O_4$ oxidation is broader, either resulting from oxidation of both Ni and Co ions or from slower electron transfer kinetics. The reverse scan for the Co_3O_4 electrode also shows a well-formed reduction peak and its shape and peak potential indicate that the kinetics of the electron transfer reaction is relatively rapid. In contrast, the reverse scan for the $NiCo_2O_4$ coating shows two broader features extending down towards the negative potential limit, again attributable to more complex electron transfer kinetics. In fact, however, several papers report voltammetry for $NiCo_2O_4$ in similar conditions [15-25] and the scans to negative potentials show significant variation and this is likely to result from different preparations. It should be recognised, however, that the exact oxidation states of the metal ions in both the as-prepared and oxidised forms cannot be determined by voltammetry.

All the peak current densities are proportional to the potential scan rate and at all scan rates the total cathodic charge equates to the charge under the oxidation peak confirming that the charge passed is limited by the availability of a species on the surface. On the other hand, the charge associated with the oxidation peak (~ 1.5 mC cm^{-2}) is small compared to that for the $1e^-$ oxidation of all the nickel and cobalt ions in the spinel contained with the film (~ 30 mC cm^{-2}). Hence, only the surface layers of the spinel particles are oxidised/reduced during potential cycling.

It can also be seen from figure 1 that the responses on the 1st and 10th cycle are very similar. With $NiCo_2O_4$, during the first 10 cycles, there is a small increase in peak heights compatible with a slight increase in surface area. Overall, however, a complete potential cycle does not change the spinel significantly; oxidation and then reduction of the surface layers is returning the spinel to its original composition and similar structure. On the other hand, oxygen evolution and reduction take place with the Ni/Co in the surface layers of the spinels in different oxidation states (oxygen evolution can be seen at potentials positive to the anodic peak while O_2 reduction occurs at negative potentials, see section 3.2). It is to be expected that during battery operation, immediately following a switch between charge and discharge, the electrode reaction will be the oxidation/reduction of the transition metal ions (rather than O_2 reduction/evolution) until the catalyst has reached the equilibrium oxidation state for the new potential. In GDE electrode structures with high loadings of the spinel catalyst, the charge in these conversions is substantial and therefore influences battery performance [12,13].

The need for a change in oxidation state of the spinel surface may be confirmed in experiments where the open circuit potentials of the spinel layers are monitored. After preparation, the open circuit potentials are ~ + 100 mV vs Hg/HgO. Figure 2 reports the open circuit potentials as a function of time following periods where oxygen is evolved or reduced. After reducing O_2 at – 200 mV for 60 s, the open circuit potentials of both spinels rather rapidly relax towards that for a freshly prepared spinel electrode, ~ + 100 mV; the oxidation state does not change between that in the prepared spinels and during O_2 reduction. In contrast, following O_2 evolution at + 650 mV for 60 s, the open circuit potentials are initially close to + 600 mV and only slowly relax back to ~ + 100 mV in the case of Co_3O_4 taking many hours. Oxygen evolution involves the spinels with their surfaces in a higher oxidation state and at open circuit the higher oxidation states of the Ni and Co ions are

reacting slowly with the electrolyte to return the spinel to its initial oxidation states. It appears that the reaction is faster with $NiCo_2O_4$ than with Co_3O_4 since the former regains an open circuit potential of ~ + 100 mV rather more rapidly.

3.2 Oxygen Evolution and Reduction

Figure 3 reports voltammograms for Co_3O_4, $NiCo_2O_4$ and Pt Black catalysed glassy carbon RDE in oxygen saturated, 1 M KOH at a temperature of 298 K. The responses at negative potentials reinforce the conclusions of an earlier paper [14]. Oxygen reduction occurs at all three catalysts and, in terms of both potential and limiting current, the activity declines in the order Pt black > $NiCo_2O_4$ > Co_3O_4. $NiCo_2O_4$ is, however, the best catalyst for O_2 evolution and this therefore somewhat improves the comparison with Pt black as a bifunctional catalyst.

In batteries and fuel cells, the electrolyte is generally 8 M KOH at an elevated temperature. Figure 4 compares voltammograms for both O_2 evolution and reduction at a $NiCo_2O_4$ catalysed glassy carbon disc electrode in 8 M KOH at 298 K and 333 K (note the current density scales for O_2 evolution and reduction are different). As expected, the potential for O_2 evolution is shifted to less positive potentials by both increasing the KOH concentration and increasing the temperature. There is a much more dramatic change in the data for O_2 reduction. The current densities for reduction in 8 M KOH are much reduced compared with those in 1 M KOH (cf. figures 3 and 4); this arises because of the much decreased solubility of oxygen, with both increasing KOH concentration and temperature, an overall factor > 25, as well as a significant decrease in the diffusion coefficient due to the higher viscosity of 8 M KOH [26-28]. Even so, comparing the responses in figures 3 and 4, shows a small positive shift for the foot of the reduction wave with increase in KOH

concentration at 298 K. Certainly, the difference in potential between O_2 evolution and reduction is decreased by the increase in KOH concentration. When the temperature is increased there are further decreases in overpotentials for both reactions confirming that operating a cell with 8 M KOH at 333 K provides a smaller potential difference between O_2 evolution and reduction in addition to providing a maximum in the electrolyte conductivity (the reason normally given for the selection of this electrolyte). Comparison of the current densities for O_2 reduction at the two temperatures is difficult because the O_2 solubility decreases while the diffusion coefficient increases with temperature.

$NiCo_2O_4$ appears to be a superior bifunctional O_2 catalyst to Co_3O_4 and was used in experiments with GDEs. We note, however, that a number of recent papers have reported studies of oxygen electrodes with nanostructured catalyst layers [25, 29-38] and those employing nanostructured Co_3O_4 powder [29-33] have reported increased catalytic activity for O_2 reduction; electrodes based on Co_3O_4 nanochains [33] are particularly active. Generally, the catalyst composition contains carbon or graphene and its influence has not been explored.

3.3 $NiCo_2O_4$ in GDEs

GDE electrodes were fabricated with $NiCo_2O_4$ as the electrocatalyst and without carbon powder using two conducting supports, stainless steel cloth and nickel foam. In all tests with GDE the electrolyte was 8 M KOH and the temperature was 333 K.

3.3.1 Stainless Steel Cloth Based GDEs

Figure 5 reports the potential vs time response from an experiment where a GDE with a $NiCo_2O_4$ powder/PTFE layer on a stainless steel cloth was cycled between O_2 reduction and O_2 evolution at three different current densities. It can be seen that at each current density, steady potentials are established for both reactions after an initial period for the change in oxidation state of the metal ions in the spinel in the electrode to occur. The experiment also confirms the conclusion from the RDE experiments; $NiCo_2O_4$ is an effective bifunctional electrocatalyst. In addition, as expected, the overpotentials for both O_2 reduction and evolution increase with current density (although there is an unknown contribution from uncompensated IR drop in these changes in potential). Table 1 reports the potentials for O_2 reduction and evolution as a function of current density as well as the difference in these potentials. This difference represents the inefficiency resulting from the oxygen electrode in a metal air battery. For example, at a current density of 10 mA cm^{-2} the potential difference is 560 mV and in a zinc/air battery this loss corresponds to ~ 34 % of the thermodynamic battery voltage..

It was further noted that even when O_2 evolution was carried out at 50 mA cm^{-2}, only a few O_2 gas bubbles were seen on the electrolyte side of the GDE; as desired the oxygen was largely evolved into the gas phase at the back of the electrode.

Moreover, this performance was achieved with a relatively low catalyst loading, ~ 20 mg cm^{-2}, compared to GDEs based on Ni foam. Unfortunately, however, the steel cloth electrodes are not entirely stable. Figure 6 reports the potential vs time response during 2 hour cycles of an electrode at 50 mA cm^{-2}; while the electrode cycles, there is a degradation in the potential for O_2 reduction after only a couple of cycles. Furthermore, above 50 mA cm^{-2} the performance of this GDE showed poor reproducibility

It should be stressed that the performance of the GDEs is critically dependent on the structure of the active layer as well the electrocatalyst. This is illustrated in figure 7 by sets of potential/time profiles from O_2 reduction/evolution cycles at three current densities for GDEs fabricated by spray coating stainless steel with a $NiCo_2O_4$/PTFE ink containing various additions of sodium sulfate as a pore former. The potential for O_2 evolution is essentially unaffected although the charge associated with the change in oxidation state of the Ni/Co ions increases with sodium sulfate content implying a greater penetration depth of electrolyte into the active layer. In contrast, the potential for O_2 reduction is greatly improved by the sodium sulfate additions; the presence of pores improves the transport of reactant gas to the active catalyst sites. The addition of 10 % Na_2SO_4 leads to a substantial positive shift in the O_2 reduction potential at all three current densities. Higher additions lead to further but smaller improvements especially at the higher current densities until with > 30 %, the electrodes become less stable (data not shown).

3.3.2 Ni Foam Based GDEs

Figure 8 reports the potential vs time response from an experiment where a GDE with a $NiCo_2O_4$ powder/PTFE layer compressed into a Ni foam was cycled between O_2 reduction and O_2 evolution at three different current densities. Again, it can be seen that at each current density, steady potentials are established for both reactions after an initial period for the change in oxidation state for the spinel surface to occur. It is also clear that this GDE design allows operation at 100 mA cm^{-2}. Similar to the stainless steel cloth GDEs, the overpotentials increase with current density, see table 1, and the potentials for both O_2 evolution at the two GDEs are not dissimilar. Again, within this GDE structure, $NiCo_2O_4$ is a

good bifunctional catalyst and it could be confirmed visually that O_2 gas is not released into the electrolyte during O_2 evolution.

A Ni foam based GDE with a $NiCo_2O_4$/PTFE active layer was cycled hourly over a 4 day period using a current density of 50 mA cm^{-2}; this corresponds to 100 cycles and figure 9 reports potential vs time response during the 10^{th} and 100^{th} cycle. It can be seen that even after 100 cycles the potential during O_2 evolution is unchanged while the potential during O_2 reduction has shifted only slightly negative. In fact, the potential change occurs slowly throughout the cycling but it is clear that this electrode cycles well. Inevitably, the GDEs constructed with a Ni foam support and current collector required much higher spinel loadings (~ 120 mg cm^{-2}) as the $NiCo_2O_4$/PTFE powder paste has the role of conducting space filler in the large pores of the foam in addition to the spinel acting as catalyst. Hence one should be cautious about the term 'catalyst loading'. At lower current densities, very similar potentials can be achieved at the stainless steel cloth GDEs despite the lower spinel loading. Also included in table 1 is data taken from experiments with a $NiCo_2O_4$ coated Ni powder/PTFE on Ni foam GDE fabricated as previously described [12,13]. This is another approach to lowering the spinel loading in the GDE as the Ni metal powder now performs the role of conducting space filler in the foam structure. The performance for O_2 evolution is very similar with the two types of foam electrodes but that for O_2 reduction is slightly worse with the Ni metal powder GDE. It is not clear whether the difference in performance results from the lower spinel loading or differences in the structure of the active layer.

The structure achieved with the compressed Ni foam GDEs, however, certainly allows operation at higher current densities and they give much more stable operation over an extended period.

4. Discussion

The results in this paper confirm earlier conclusions that $NiCo_2O_4$ is better than Co_3O_4 as an electrocatalyst for O_2 reduction [14]. It was shown in this earlier paper that in addition to a less negative potential for O_2 evolution, unlike Co_3O_4, $NiCo_2O_4$ promotes the full $4e^-$ reduction of oxygen. $NiCo_2O_4$ is also a better catalyst than Co_3O_4 for O_2 evolution making it a much superior bifunctional catalyst. Pt black may be slightly better than $NiCo_2O_4$ but it is, of course much more expensive especially when used in a form free from carbon support. Since an objective was a bifunctional catalyst free of precious metal, $NiCo_2O_4$ was the only material chosen for fabrication into GDE.

Three types of GDE have been fabricated based on different current collector materials and presentation of the spinel. The goal has always been threefold (a) a low difference in potentials for O_2 reduction and evolution (b) a long cycle life and (b) delivery of the gas to the back of the GDE during O_2 evolution, with these targets to be achieved at the highest possible current density. The performance of GDEs depends on additional factors than at RDEs. The structure of the active layer in the GDE must allow supply and removal of O_2 to/from the active sites as well as the stable presentation of the electrolyte phase to the active sites. Current distribution in the active layer is also important. Thus it is never certain whether a decline in performance in the bifunctional GDE with time results from changes in electrocatalyst behaviour or changes in the electrode structure (eg. loss of current path between catalyst sites and current collector, creep of the electrolyte through the active layer).

In terms of long term performance, the GDE electrodes based on Ni foam are certainly superior to those based on steel cloth. On the other hand, the fabrication of the GDE based on Ni foam is more difficult to scale up from the 1 cm^2 used here to the fraction of 1 m^2 desirable for a practical battery. Also the fabricated GDEs are thicker and less flat than conventional GDEs and this imposes limitations on the way that the GDE can be engineered

into a practical flow cell design. The electrodes based on $NiCo_2O_4$ powder show better performance that those based on $NiCo_2O_4$ coated Ni metal powder, but this requires significantly more spinel. Whether the difference reflects difference in catalyst behaviour or structure of the GDE is not known.

5. Acknowledgement

Part of this work was carried out using financial support by the European Commission (Theme 2010.7.3.1) Energy Storage Systems for Power Distribution Networks, Grant Agreement No. 256759, and this support is gratefully acknowledged. TS acknowledge the receipt of a studentship from the Ministry of National Education, Republic of Turkey.

References

1. K. Kinoshita, *Electrochemical Oxygen Technology*, John Wiley & Sons Inc. 1992.
2. M. Hamdani, R.N. Singh and P. Chartier, Co_3O_4 and Co-based spinel oxides bifunctional oxygen electrodes, *Int. J. Electrochem. Sci.,* **5** (2010) 556 – 577.
3. L. Jörissen, Bifunctional oxygen/air electrodes, *J. Power Sources,* **155** (2006) 23-32.
4. V. Nikolova, P. Iliev, K. Petrov, T. Vitanov, E. Zhecheva, R. Stoyanova, I. Valov and D. Stoychev, Electrocatalaysts for bifunctional oxygen/air electrodes, *J. Power Sources,* **185** (2008) 727-733.
5. V. Neburchilov, H. Wang, J.J. Martin and W. Qu, A review on air cathodes for zinc-air fuel cells, *J. Power Sources,* **195** (2010) 1271-1291.
6. X-Z. Yuan, W. Qu, X. Zhang, P. Yao and J. Fahlman, Spinel $Ni_xCo_{2-x}O_4$ as a bifunctional air electrode for zinc-air batteries, *ECS Trans*., **45(29)** (2013) 105-112.
7. P.N. Ross and H.Sokol, The corrosion of carbon black anodes in alkaline electrolyte. Part I. Acetylene black and the effect of cobalt catalyzation, *J. Electrochem. Soc.*, **131** (1984) 1743-1750.
8. N. Staud and P.N. Ross, The corrosion of carbon black anodes in alkaline electrolyte. Part II. Acetylene black and the effect of oxygen evolution catalysts on corrosion, *J. Electrochem. Soc.*,**133** (1986) 1079-1084.
9. P.N. Ross and M. Sattler, The corrosion of carbon black anodes in alkaline electrolyte. Part III The effect of graphitization on the corrosion resistance of furnace blacks, *J. Electrochem. Soc.*,**135** (1988) 1464-1470.
10. N. Staud, H. Sokol and P.N Ross, The corrosion of carbon black anodes in alkaline electrolyte. Part IV Current efficiencies for oxygen evolution from oxide impregnated graphitised furnace blacks, *J. Electrochem. Soc.*,**136** (1989) 3570-3576.

11. S. Műller, F. Holzer, H. Arai and O.Haas, A study of carbon-catalyst interaction in bifunctional air electrodes for zinc-air batteries, *J. New Mater. Electrochem Systems*, **2** (1999) 227-232.

12. X. Li, D. Pletcher, A.E. Russell, F.C. Walsh, R.G.A. Wills, S.F. Gorman, S.W.T. Price and S.J. Thompson, A Novel Bifunctional Oxygen GDE for Alkaline Batteries, *Electrochem. Commun.,* **34** (2013) 228-231.

13. S.W.T. Price, S.J. Thompson, X. Li, S.F. Gorman, D. Pletcher, A.E. Russell, F.C. Walsh, R.G.A. Wills, The Fabrication of a Bifunctional Oxygen GDE without Carbon Components for Alkaline Secondary Batteries, *J. Power Sources***, 259** (2014) 43-49.

14. D. Pletcher, S.W.T. Price, A. E. Russell, T. Sönmez and S. J. Thompson, Voltammetric studies of Oxygen Reduction at the Spinels Co_3O_4 and $NiCo_2O_4$, Electrochim. Acta, submitted PA-15-03245.

15. A. Carugati, G.Lodi and S. Trasatti, Effect of Solution pH on the surface properties of $NiCo_2O_4$ electrodes, *J. Electroanal. Chem.,* **143** (1983) 419-423.

16. J. Haenen, W. Visscher and E. Barendrecht, Characterisation of $NiCo_2O_4$ electrodes for O_2 evolution. Part III Aging phenomena of $NiCo_2O_4$ electrodes, *J. Electroanal. Chem.,* **208** (1986) 323-341.

17. M. El Baydi, S.K. Tiwari, R.N. Singh, J-L. Rehspringer, P. Chartier, J.F. Koenig and G. Poillerat, High specific surface area $LaNiO_3$ and $NiCo_2O_4$ via sol-gel type routes for oxygen electrocatalysts in alkaline media, *J. Solid State Chem.,* **116** (1995) 157-169.

18. P. Nkeng, J.F. Koenig, J.L. Gautier, P. Chartier and G. Poillerat, Enhancement of surface area of Co_3O_4 and $NiCo_2O_4$ electrocatalysts prepared by spray pyrolysis, *J. Electroanal. Chem.*, **402** (1996) 81-89.

19. I. Nikolov, R. Darkaoui, E. Zhecheva, R. Stoyanova, N. Dimitrov and T. Vitanov, Electrocatalytic activity of spinel related cobaltites $M_xCo_{3-x}O_4$ (M = Li, Ni, Cu) in the

oxygen evolution reaction, *J. Electroanal. Chem.,* **429** (1997) 157-168.

20. B. Chi, J. Li, Y. Han and Y. Chen, Effect of temperature on the preparation and electrocatalytic properties of a spinel $NiCo_2O_4$/Ni electrode, *Int, J. Hydrogen Energy,* **29** (2004) 605-610.
21. B. Chi, H. Lin, J. Li, N. Wang and J. Yang, Comparison of three preparation methods of $NiCo_2O_4$, *Int, J. Hydrogen Energy,* **31** (2006) 1210-1214.
22. Y.Q. Wu, X.Y. Chen, P.T. Ji and Q.Q.Zhou, Sol-gel approach for controllable synthesis and electrochemical properties of $NiCo_2O_4$ crystals as electrode material for application in supercapitors, *Electrochim. Acta,* **56** (2011) 7517-7522.
23. N. Padmanathan and S. Selladurai, Solvothermal synthesis of mesoporous $NiCo_2O_4$ spinel oxide nanostructure for high performance electrochemical capacitor electrode, *Ionics,* **19** (2013) 1535-1544.
24. M.U.A Prathap and R. Srivastava, Synthesis of $NiCo_2O_4$ and its application in the electrocatalytic oxidation of methanol, *Nano Energy,* **2** (2013) 1046-1053.
25. J. Shen, X. Li, N. Li and M. Ye, Facile Synthesis of $NiCo_2O_4$-reduced graphene oxide nanocomposites with improved electrochemical properties, *Electrochim. Acta,* **141** (2014) 126-135.
26. K.E. Gubbins and R.D. Walker, The solubility and diffusivity of oxygen in electrolytic solutions, *J. Electrochem. Soc.,* **112** (1965) 469-472.
27. R.E. Davis, G.L. Horvath and C.W. Tobias, The solubility and diffusion coefficient of oxygen in potassium hydroxide solutions, *Electrochim. Acta,* **12** (1967) 287-297.
28. D. Zhang, J.F. Wu, T. Okajima, F. Kitamura and T. Ohsaka, Hydrodynamic chronocoulometric estimation of diffusion coefficients and saturated concentrations of dioxygen in KOH solutions, *Indian J. Chem.,* **42A** (2003) 801-806.
29. Y. Liang, Y. Li, H. Wang, J. Zhou, J. Wang, T. Regierand H. Dai, Co_3O_4 nanocrystals on

graphene as a synergistic catalyst for oxygen reduction reaction, Nature Mater., 10 (2011) 780-786.

30. J. Xu, P. Gao, and T.S. Zhao, Non-precious Co_3O_4 nanorod electrocatalyst for oxygen reduction reaction in anion-exchange membrane fuel cells, Energy Environ. Sci, 5 (2011) 5333-5339.
31. Y.J. Sa, K. Kwon, J.Y.Cheon, F. Kleitz and S.H. Joo, Ordered mesoporous Co_3O_4 spinels as stable bifunctional, noble metal free oxygen electrocatalysts, J. Mater. Chem. A, 1 (2013) 9992- 10001.
32. F. Kong, Synthesis of rod and beadlike Co_3O_4 and bifunctional properties as air/oxygen electrode materials, Electrochim. Acta, 68 (2012) 198-201.
33. P.W. Menezes, A. Indra, D. González-Flores, N.R. Sahraie, I. Zaharieva, M. Schwarte, P. Strasser, H. Dau and M. Driess, High-performance oxygen redox catalysis with multifunctional cobalt oxide nanochains: morphology-dependent activity, ACS Catalysis, 5 (2015) 2017-2027.
34. C. Jin, F. Lu, X. Cao, Z. Yang and R. Yang, Facile synthesis and excellent electrochemical properties of $NiCo_2O_4$ spinel nanowire arrays as bifunctional catalyst for the oxygen reduction and evolution reaction, J. Mater. Chem. A, 1 (2013) 12170-12177.
35. D.U. Lee, B. Kim and Z. Chen, One-pot synthesis of mesoporous $NiCo_2O_4$ nanoplatelet and graphene hybrid and its oxygen reduction and evolution activities as an efficient bi-functional electrocatalyst, J. Mater. Chem. A, 1 (2013) 4752-4762.
36. Z-Q. Lui, Q-Z. Xu, J-Y. Wang, N. Li, S-H. Guo, Y-Z. Su, H-J. Wang, J-H. Zhang and S. Chen, Facile hydrothermal synthesis of urchin-like $NiCo_2O_4$ spheres as efficient electrocatalysts for oxygen reduction reaction, Int. J. Hydrogen Energy, 38 (2013) 6657-6662.
37. M. Prabu, K. Ketpang and S. Shanmugam, Hierarchical nanostructured $NiCo_2O_4$ as an

efficient non-precious metal catalyst for rechargeable zinc-air batteries, Nanoscale, 6 (2014) 3173-3181.

38. D.U. Lee, B.J. Kim and Z. Chen, One-pot synthesis of a mesoporous $NiCo_2O_4$ nanoplatelet and graphene hybrid and its oxygen reduction and evolution activities as an efficient bi-functional electrocatalyst, J. Mater. Chem. A, 1 (2013) 4754-4762.

Legends for Figures

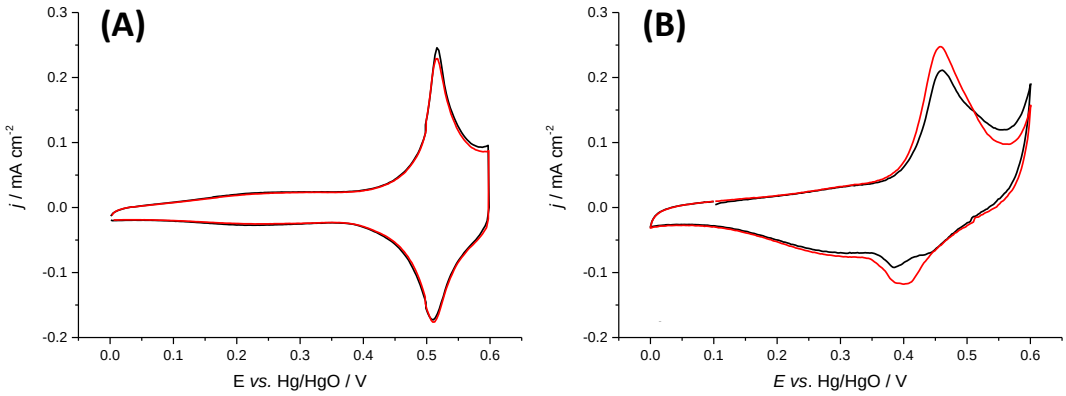

Figure 1 Cyclic voltammograms - 1st (black) and 10th cycles (red) for (A) Co_3O_4 and (B) $NiCo_2O_4$ layer in 1 M KOH. Temperature 298 K. Potential scan rate 10 m V s^{-1}.

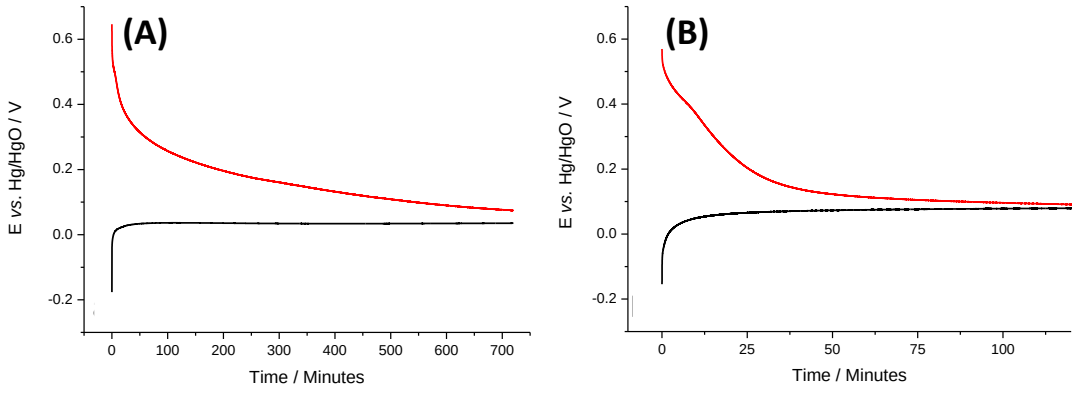

Figure 2 Open circuit potential as a function of time after a 60 s period of oxygen evolution (red curves) or oxygen reduction (black curves). Catalyst coated glassy carbon discs (A) Co_3O_4 and (B) $NiCo_2O_4$. Oxygen saturated, 1 M KOH. Temperature 298 K.

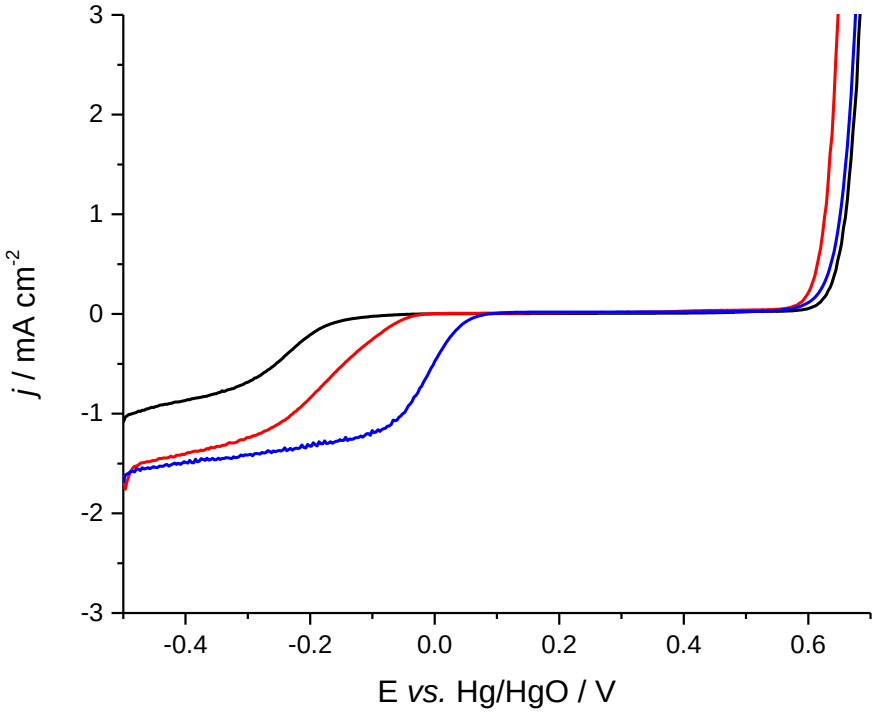

Figure 3 Voltammograms for Co_3O_4 (black), $NiCo_2O_4$ (red) and Pt black (blue) catalysed glassy carbon RDE in oxygen saturated, 1 M KOH. Temperature 298 K. Potential scan rate: 1 mV s^{-1}.

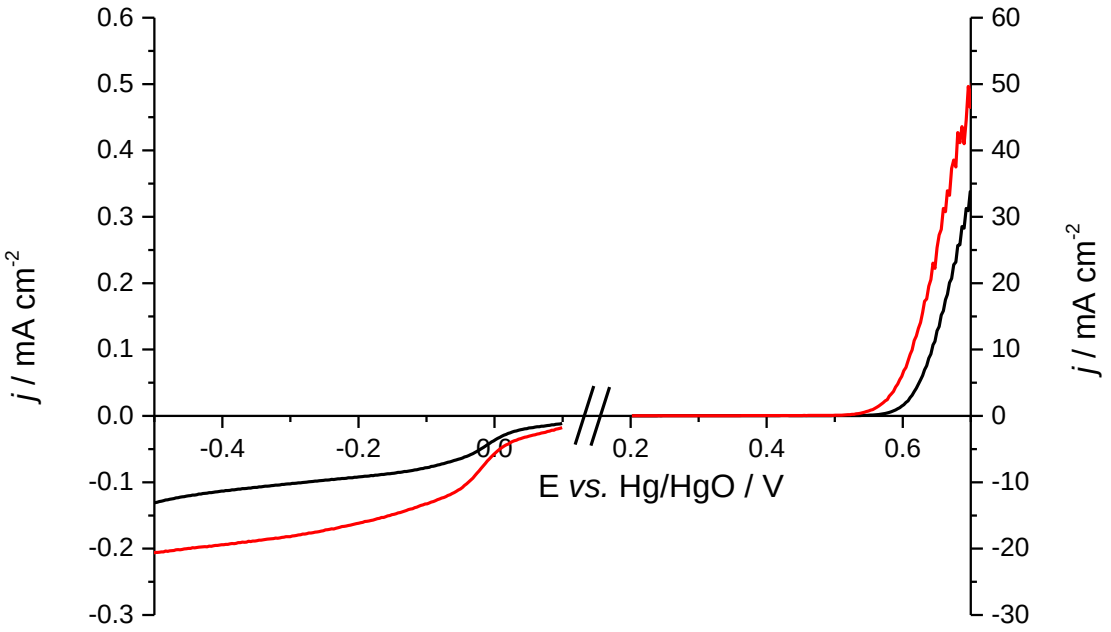

Figure 4 Voltammograms for O_2 reduction and evolution at a $NiCo_2O_4$ catalysed glassy carbon RDE in 8 M KOH at temperatures of 298 K (black) and 333 K (red). Note the different current density scales for O_2 reduction and evolution. Reduction currents were recorded at 900 rpm and oxidation current at 400 rpm.

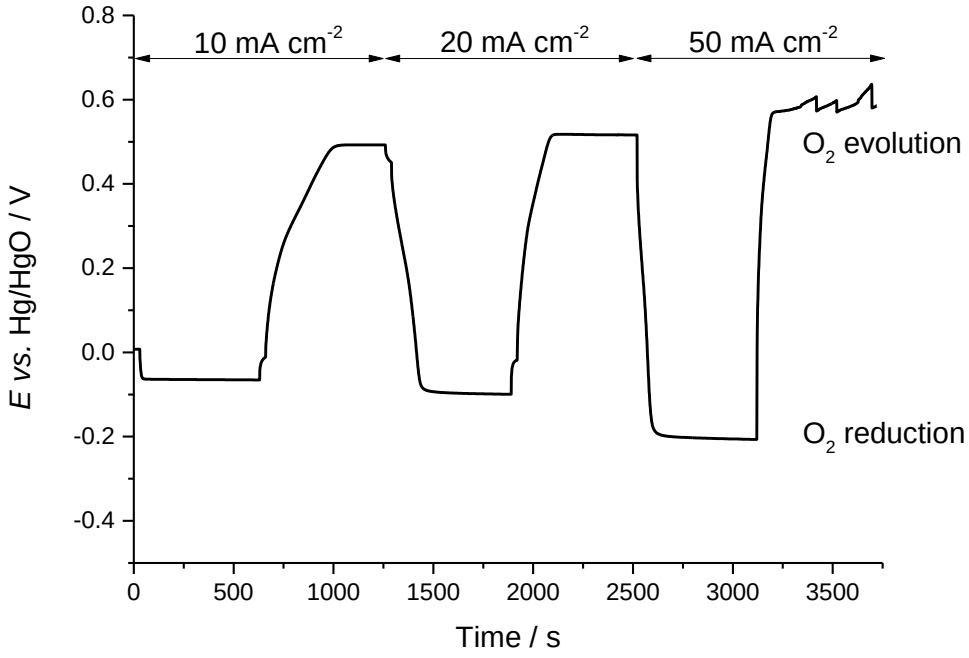

Figure 5 Potential vs time response from an experiment where a fresh GDE with a $NiCo_2O_4$ powder/PTFE layer on a stainless steel cloth was cycled between O_2 reduction and O_2 evolution. 8 M KOH. Temperature 333 K. Sodium sulphate was present in the catalyst ink to enhance pore formation.

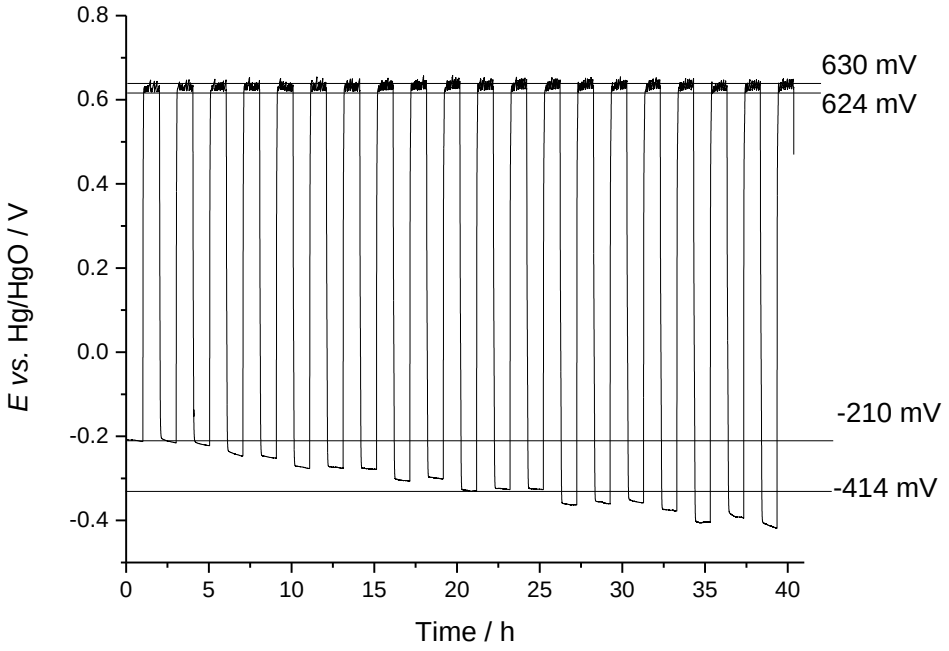

Figure 6 Potential as a function of time during cycling the current density between O_2 reduction and O_2 evolution using a steel cloth based GDE and a current density of 50 mA cm^{-2}. 8 M KOH. Temperature 333 K. Sodium sulphate was present in the catalyst ink to enhance pore formation.

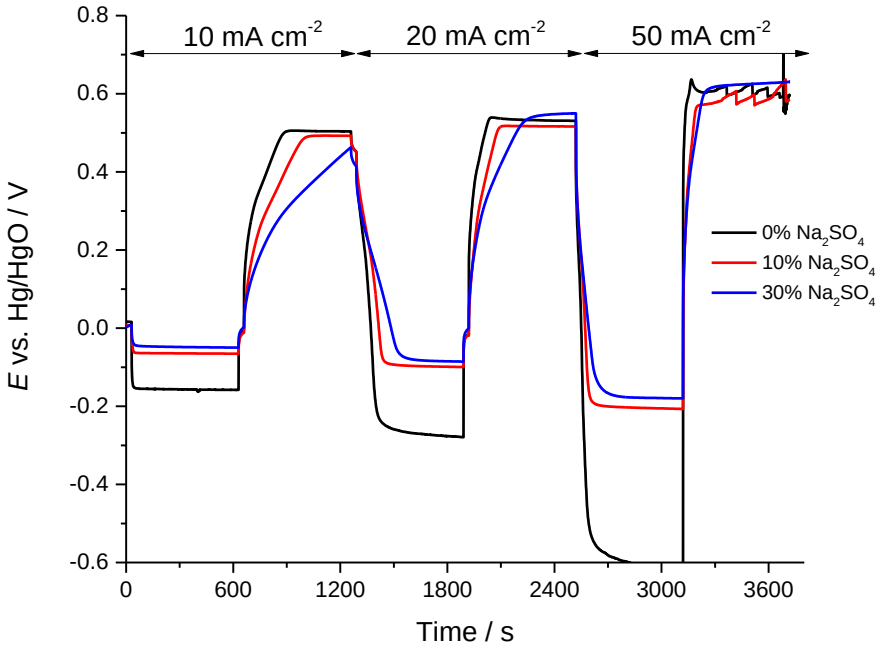

Figure 7 Potential as a function of time during cycling the current density between O_2 reduction and O_2 evolution using a stainless steel cloth based GDE prepared by spray coating with a $NiCo_2O_4$ powder/PTFE ink with various additions of Na_2SO_4; 0 % (black), 10 % (red) and 30 % (blue). With each GDE, the current densities are 10, 20 and 50 mA cm^{-2}. 8 M KOH. Temperature 333 K.

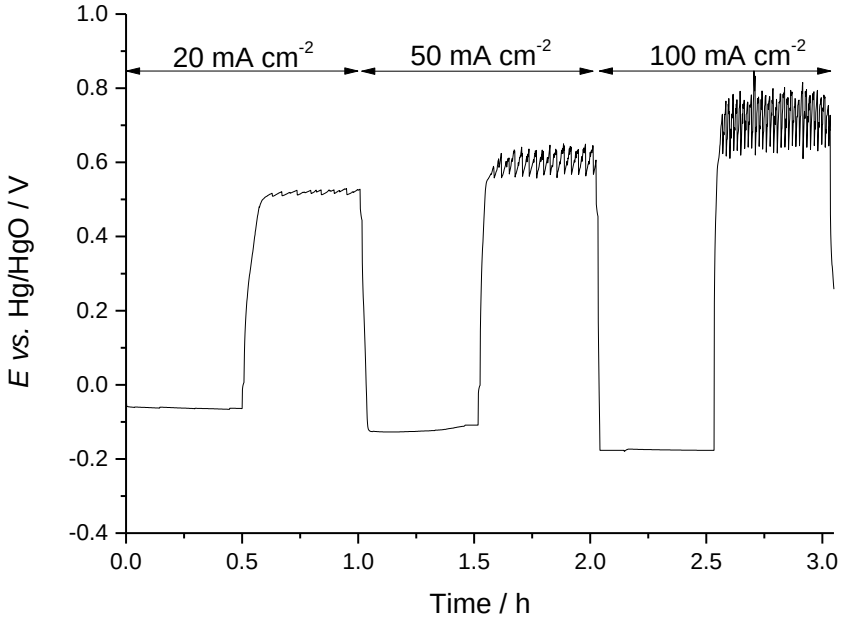

Figure 8 Potential as a function of time during cycling the current density between O_2 reduction and O_2 evolution using a Ni foam based GDE with a $NiCo_2O_4$ powder/PTFE active layer and current densities of 20, 50 and 100 mA cm^{-2}. 8 M KOH. Temperature 333 K.

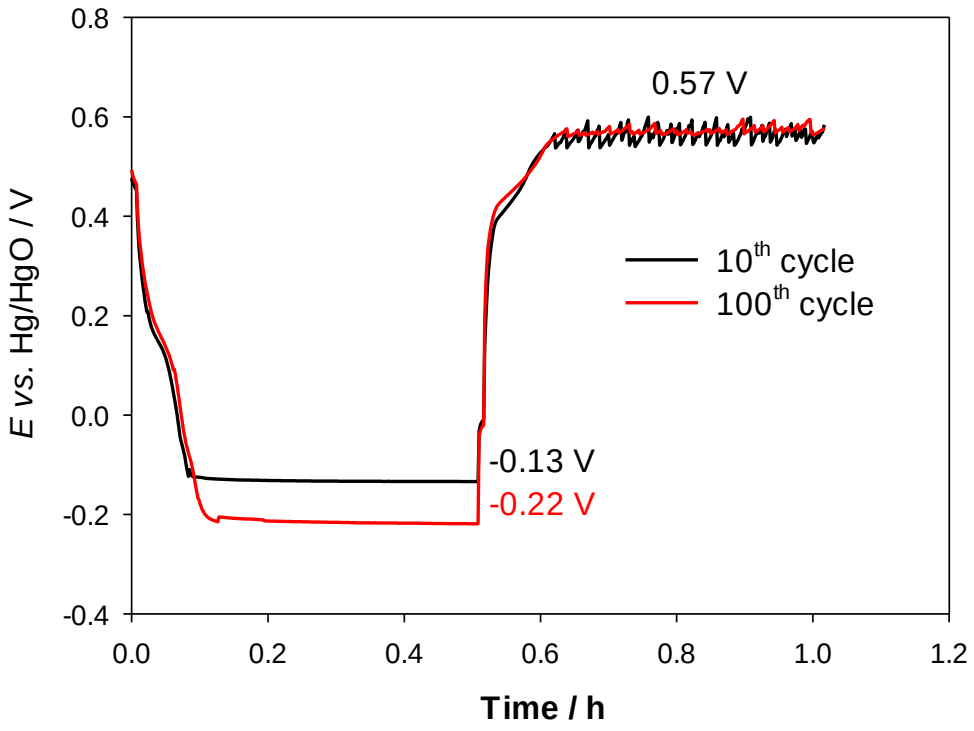

Figure 9 Comparison of the potential vs time responses during the 10st (black) and 100th (red) cycle of a Ni foam based GDE with a $NiCo_2O_4$ powder/PTFE active layer. Current density 50 mA cm^{-2}. 8 M KOH. Temperature 333 K.

Table 1 Potentials as a function of current density for GDEs cycled between O_2 reduction and evolution and differences in potentials for the oxygen electrode on charge and discharge. 8 M KOH, Temperature 333 K**.**

Type of GDE	j = 20 mA cm^{-2}			j = 50 mA cm^{-2}			j = 100 mA cm^{-2}		
	E vs Hg/HgO/mV		ΔE/mV	E vs Hg/HgO/mV		ΔE/mV	E vs Hg/HgO/mV		ΔE/mV
	O_2 reduction	O_2 evolution		O_2 reduction	O_2 evolution		O_2 reduction	O_2 evolution	
$NiCo_2O_4$ powder /PTFE on stainless steel cloth	-100	515	615	-204	596	800			
$NiCo_2O_4$ powder /PTFE on Ni foam	-60	520	580	-120	580	700	-180	660	840
$NiCo_2O_4$ coated Ni powder /PTFE on Ni foam	-105	570	575	-145	605	750	-260	650	910